The Implementation of Water Loop Analysis for Concentrated Solar Thermal Application

Walter Parker

Mentor: Vinod Narayanan, Ph.D.
Mechanical Engineering

Abstract

Concentrated solar thermal is a renewable method of electric power generation in which a traditional thermodynamic cycle is driven by solar heat. Solar energy is concentrated by a dish or a heliostat field, and the high density thermal input is incident on a receiver. A receiver takes concentrated sun energy and transfers it to a working fluid. The hot working fluid is then routed for power generation. In this project, the goal is to develop a method to characterize the efficiency of two types of solar thermal heat concentration setup. One where the working fluid is water and the other for which the working fluid is supercritical Carbon Dioxide (sCO_2). For this project the primary focus will be on the water setup. A 7m parabolic solar dish is being used to concentrate solar energy incident on the receiver. Two methods were used to assess the efficiency, first one is to examine how much solar energy was extracted from the receiver to the water. The second method uses a Sandia PHLUX program for solar distribution incident on the surface of the receiver. A MATLAB model of this loop's components and their performance is created using thermodynamics and fluid mechanics calculation to size the equipment. A Post processing MATLAB model was developed to examine the solar energy incident on the receiver. Perturbation uncertainty analysis was used to assess uncertainty in the amount of solar incident on the receiver. Using the information from both methods efficiency is calculated.

Nomenclature:

Symbol	Name of Variable	Units
c_p	Specific heat capacity of the working fluid	$\dfrac{J}{kg\ K}$
D	Diameter of the tubing for water loop	m
ϵ	Surface Roughness of piping	m
f	Friction factor of tubing	-
g	Gravity	$\dfrac{m}{s^2}$
gpm	Gallons per minute	$\dfrac{gallons}{min}$
h	Heat transfer coefficient microchannel pin	$\dfrac{W}{m^2\ K}$
h_f	Frictional Head loss	m
k_f	Thermal Conductivity of working fluid	$\dfrac{W}{m\ K}$
L	Length of the tubing	m
m	Flowrate of working fluid	$\dfrac{kg}{s}$

m_{hx}	Flowrate necessary through heat exchanger	$\dfrac{kg}{s}$
η_{carnot}	Carnot Efficiency	-
$\eta_{receiver}$	Receiver Efficiency	-
P_1	Pressure at State 1	Pa
P_2	Pressure at State 2	Pa
ΔP_{12}	Pressure difference between state 1 and state 2	Pa
ΔP_{hx}	Pressure drop through the heat exchanger	Pa
ρ	Density of the working fluid	$\dfrac{kg}{m^3}$
q_{fluid}	Energy Transferred to the working fluid	W
$q_{incident}$	Solar Energy Incident on receiver surface	W
Re	Reynolds Number	-
$sCO2$	Supercritical Carbon Dioxide	-
T_c	Temperature of the cold source	K
T_h	Temperature of the hot source	K
T_{in}	Temperature of incoming fluid to the receiver	K
T_{out}	Temperature of exiting fluid from the receiver	K
ΔT	Temperature difference between the receiver	K
V_1	Velocity at State 1	$\dfrac{m}{s}$
V_2	Velocity at State 2	$\dfrac{m}{s}$
z_1	Height at State 1	m
z_2	Height at State 2	m

Introduction:

The need for cleaner energy has been growing in the past decade. This need stems from the fact that countries around the world have a heavy dependence on fossil fuels and natural gas for power. This heavy dependence has created a rise in CO_2, particulate matter, and other pollutants, which are major contributors towards global warming. With a goal of reducing the

amount of CO_2 being produced, the US Department of Energy started the SUNSHOT initiative [1]. Sunshot's mission was to enable production of low cost electricity using solar energy. A common way of producing electricity through solar energy is by using photovoltaic solar panels which takes sun light and converts it directly to electricity using the photovoltaic effect. Another method is called concentrated solar thermal power generation which is a renewable process of electric power generation in which a traditional thermodynamic cycle is driven by solar heat. Solar energy can be concentrated at the focal point of a parabolic dish or trough. At the focal area, concentrated solar energy is transferred to a working fluid in a device called a solar thermal receiver. The hot working fluid from the receiver is either stored for later use or directly or indirectly used by a turbine to produce electricity. Concentrated solar thermal power generation could potentially provide a baseload supply of power to a region if coupled correctly with thermal storage. This form of power generation can be used ultimately to lead this country in a direction that is less dependent on fossil fuels and natural gas as a source of power and heating.

Concentrated Solar Thermal power generation has been around since the 70s and has constantly been improved to obtain higher overall solar to electricity efficiency. One way to improve the overall efficiency is by changing the working fluid through the solar thermal receiver, which may allow higher temperatures that could potentially result in higher Carnot efficiency. Molten salt is one common type of fluid used in the receivers and reaches temperatures up to around 600 degrees Celsius [2].

The second method of improving the overall efficiency of concentrated solar thermal power generation is by designing new types of receiver that can maximize the heat transfer occurring between the receiver and the fluid. Different types of receivers have been created to help address the issue of improving the efficiency of solar thermal heat concentration. One type of receiver is the solid particle-based receiver developed by Sandia National Laboratory. It uses ceramic type particles as the heat transfer media and results have shown that in this technique the media has been able to reach temperatures over 1000 degrees Celsius helping with the overall efficiency enhancement [2]. This type of receiver design is useful because the particles provides a direct way of storing the energy for later uses. Other type of receiver includes liquid-based receivers and gas-based receivers which have been developed to address this efficiency issue.

A microchannel receiver, developed by Oregon State University and UC Davis, is an example of a gas-based receiver which has potential to improve receiver efficiency by implementing advantages of microchannel technology. With the growing need for cleaner energy, novel microchannels design can help reduce the cost of building concentrated solar thermal power generation plants; since this new microchannel receiver will achieve higher amount of heat transfer within a smaller design, thus reducing the cost of the overall concentrated solar thermal system while also improving the efficiency.

In lab results with the small receiver with supercritical carbon dioxide (sCO_2) as the working fluid, data have shown thermal efficiencies more than 90 percent [2] at heat fluxes as high as 100 W/cm^2. Due to the larger surface area for heat loss (5cm x 5cm) relative to the incident heat flux area on the receiver (2cm x 2cm), heat loss corrections had to be made to estimate the thermal efficiency.

The goal of the work presented in this report is to further advance the microchannel receiver technology by evaluating its performance on a larger scale receiver and under real operating conditions. A larger-scale 8cm x 8cm receivers, designed and fabricated in earlier work [3], will be used in the experiments. The receiver has been static-pressure-tested at the design operating temperature of 650 C and 200 bar internal pressure to verify its structural integrity. To characterize this receiver, a seven-meter parabolic dish, installed at UC Davis by the members of the Solar Thermal and Energy Enhancement Laboratory (*STEEL*), will be used. Furthermore, the sCO$_2$ loop, built by members of the *STEEL* group, is then used to characterize the performance of the 8cm x 8cm receiver. To determine the efficiency of the receiver, the amount of concentrated energy incident on the receiver and energy transferred to the working fluid needs to be first characterized. The goal of this paper is to develop experimental and data analysis methods to determine the receiver efficiency. The methods have been demonstrated on a water receiver. The amount of concentrated energy incident on the receiver surface will be determined using Sandia National Laboratory's PHLUX mapping program. The amount of energy extracted by the working fluid from the receiver will be determined using collected data from thermocouples and flowmeter. Using both values from each process, the receiver efficiency can be assessed.

Test Facilities Design

To characterize the receiver efficiency performance, a test loop was designed and constructed to monitor a commercial base receiver seen in Fig. 1 with water as the heat transfer fluid. The same method used to analyze the efficiency of the commercial base receiver would be used to analyze the efficiency of the microchannel receiver. A closed loop was developed with water as the working fluid in order to characterize the commercial receiver efficiency (purpose 1). This loop will also be used as one of the cooling stages for the sCO$_2$ loop. The sCO$_2$ fluid needs to reject enough heat to be condensed back to liquid state to be able to repeat the closed loop process (purpose 2). The nominal heat rejection in the water loop is anticipated to be ~30 kW (40 hp). The second purpose is to analyze the commercial receiver performance at the focal point, which expects to receive around 28.5 kW (38.2 hp). The schematic of the water loop can be seen in Fig 1.
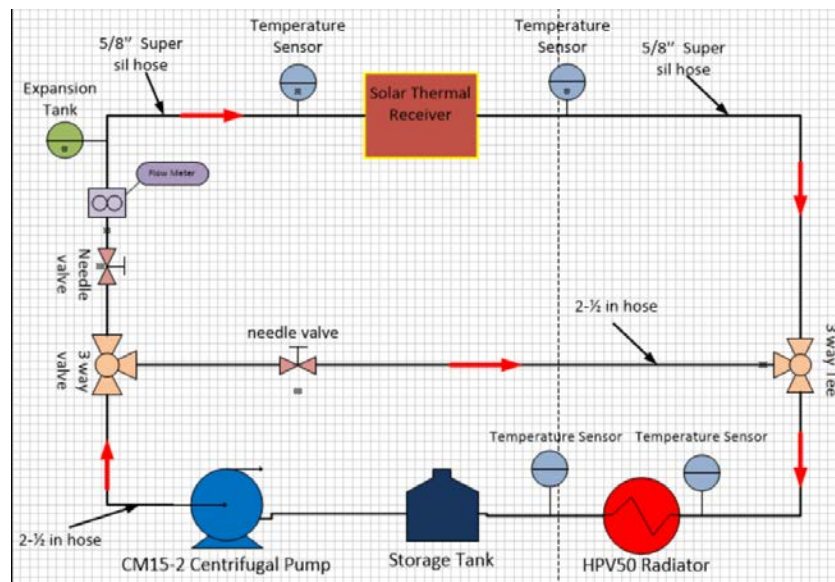
Figure 1: Schematic of Water Loop

The diagram in Fig. 1 shows the direction of the flow. The centrifugal pump pushes 166.36 liter/min (43.95 gallon/min) of fluid through a three-way valve where 143.27 liter/min (37.85 gallon/min) gets diverted through a bypass loop and 23 liter/min (6.10 gallon/min) travels through the receiver. The fluid is pushed through a needle valve and a flow meter, it passes through an expansion tank that regulates the pressure before entering the commercial receiver. After passing through the receiver the fluid has passed several measuring devices such as the flow meter to monitor the mass flow rate of the fluid, and thermocouples to measure the inlet and exit temperatures. These measurements, along with the specific heat of the fluid, were used for determining the amount of solar energy being added to the fluid. Upon exiting the receiver, the fluid is directed through a one-way valve to prevent backflow of the working fluid. After passing the one-way valve the working fluid merges with the bypass fluid and enters into an air-cooled radiator where temperatures are recorded at the inlet and exit ports and eventually the flow goes back to the storage tank repeating the process.

The main components that were essential and needed to be properly down selected for the loop was the flow meter to keep track of the fluid flow, a centrifugal pump to circulate the fluid through the loop (Fig. 2), a commercial based receiver used for transferring heat incident on the surface to the working fluid (Fig 3) and radiator for cooling the fluid to repeat the process (Fig 4). When designing this loop, thermodynamics and fluid mechanic calculation were performed to assess the total amount of solar energy needed to be removed, pressure drop through the lines, and the necessary flowrate. Several aspects needed to be considered in the design of the loop. In the design the radiator requires a larger fluid flow rate to reject the expected amount of incoming heat from the solar receiver, this is a problem because the necessary flow rate for the radiator is significantly larger than the required flow rate to the receiver. The flow rate for the receiver could not be large because larger flow rate causes the temperature difference between inlet and exit become very close to each other and consequently the uncertainty in the measurement goes higher. To compensate for the flowrate in the receiver and the flowrate of the radiator a bypass

6

loop was implemented to divert the necessary fluid using a three-way valve to satisfy the receiver's condition. The bypass loop would then reconnect with the returning flow from the receiver to travel through the radiator.

Figure 2: Centrifugal Pump

Figure 3: Commercial Solar Receiver

Figurer 4: Radiator

To characterize the specification of the equipment, pressure drop and flow rate in the loop, a MATLAB code was created. Based on the dimensions of the piping, the material properties, surfaces roughness of the tubing, information extracted from performance curves of the radiator and data on the commercial receiver [4], the total pressure drop was assessed for the closed loop. To analyze the loop performance, Bernoulli equation was used to calculate the amount of pressure drop through the loop. Bernoulli equation with frictional head loss is defined as

Equation 1: $z_1 + \frac{P_1}{\rho g} + \frac{V_1^2}{2g} = z_2 + \frac{P_2}{\rho g} + \frac{V_2^2}{2g} + h_f$

Simplifying the Bernoulli equation in terms of the change in pressure the new equation is defined as

Equation 2: $\Delta P_{12} = \rho g * (z_1 - z_2) + \rho g * h_f$ with $h_f = f\frac{L}{D} * \frac{V_2}{2g}$

For preliminary calculation, to model the MATLAB program, the potential temperature difference between the inlet and exit temperature was fixed for the working fluid. Secondly the maximum amount of solar energy incident on the receiver for the water loop setup was set which was provided by the manufacturer of the parabolic dish [5]. Using the temperature difference and the maximum amount of solar energy incident possible on the receiver, an approximate value for the maximum flowrate through the receiver was obtained. With this flow rate the velocity for the fluid through the receiver was assessed, the equation used to determine the flowrate is defined as

Equation 3: $m\_dot = \frac{q_{fluid}}{c_p \Delta T}$

Using these preliminary values helped to size the appropriate radiator and centrifugal pump. One constraint with the design is that the temperature had to be fixed in order to get initial calculations which limited the accuracy of potential flowrates. Once construction of the test loop was finished, the actual flowrate and inlet and exit temperature was measured using a turbine flowmeter and T-type thermocouples respectively. These values gave accurate measurements for heat transferred to the fluid in the commercial receiver and the flowrates.

With equation 1 the total amount of pressure drop in the loop is assessed. To calculate the frictional head loss the friction factor was needed. The friction factor (f) is a function of Reynolds number, tubes inner diameter, and surface roughness of the tube. Using the explicit form of friction factor relation (Haaland's equation), the friction factor can be defined as

Equation 4: $\frac{1}{f^{1/2}} = -1.8 * \log(\frac{6.9}{Re} + \left(\frac{\frac{\epsilon}{D}}{3.7}\right)^{1.11})$

Once the friction factor was obtained, Equations 1 and 2 were used to calculate the total pressure drop. To properly size the radiator the maximum expected heat input that needed to be removed from the working fluid was used, which was anticipated to be ~30 kW (40 HP). Since the amount of heat rejected from the radiator was dependent on the flow rate, a performance curve was created using excel to track how the flow rate varied with the amount of rejected heated seen in Fig. 5. This performance curve was created by using information provided by the manufacture [6]. This data included information on how the radiators functioned at different operating

conditions and what its capabilities were. From these operating conditions it was possible to plot them on excel to evaluate the trend.
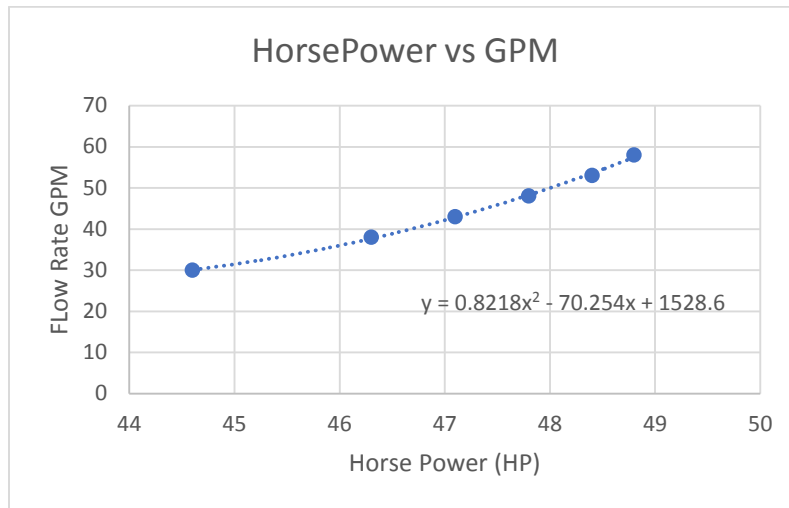

Figure 5: Radiator plot of the Flow Rate as a function of Horse Power

From the performance curve, a curve fit equation was created with excel that showed required flow rate as a function of the heat input to the working fluid which is in the form of,

Equation 5: $m_{hx} = 0.821 * (q_{fluid})^2 - 70.254 * q_{fluid} + 1528.6$

Knowing how large of a flow rate was needed for the radiator to properly work, helped to determine how much flow rate was needed for each region and what amount of flowrate needed to be diverted. The next parameter calculated for the radiator was the pressure drop through it. Using the same operating conditions provided by the manufacture a second performance curve was created in excel that detailed how flow rate affected the pressure drop within the radiator seen in Fig. 6.
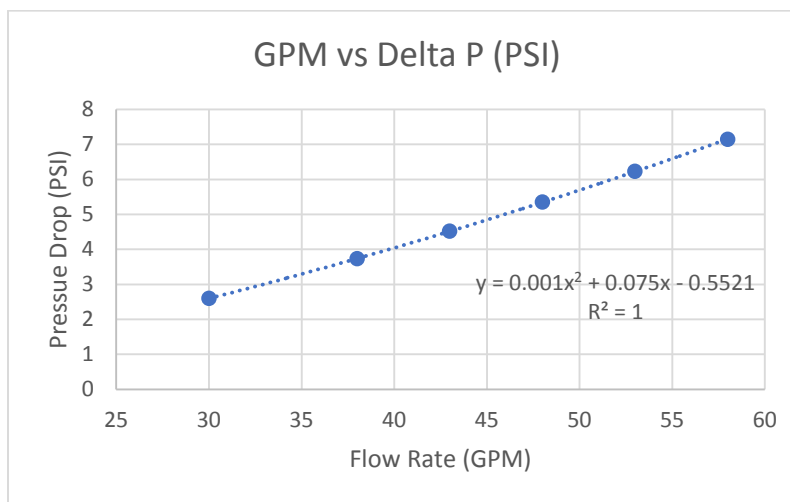

Figure 6: Radiator plot Pressure Drop as a function of Flow Rate

The UC Davis McNair Scholars Journal

From this performance curve an equation was generated that showed pressure drop through the radiator as a function of flow rate which was defined as

Equation 6: $\Delta P_{hx} = .001(m_{hx})^2 + .075 * m_{hx} - 0.5521$

Both Equation 5 and 6 generated for the radiator was implemented into the MATLAB code to determine which radiator option was the best choice. After detail analysis of the radiators performances curves, the best radiator for the situation was the EMMEGI HPV50-1NS-JE-22 heat exchanger with a 1 phase 115-230v 60Hz NEMA motor [6]. This radiator can remove 36.5 kW (48.8 HP) at max flow rate of 219.5 liters/min (58 gallons/min) for the water as working fluid at pressure drop of 49.29 kPa (7.15 PSI). Using equations 1 through 5 in the MATLAB code and varying the amount of heat input, tube diameter, and the flow rate to see how that effects the pressure drop and performance, the total amount of pressure drop through the system is assessed allowing for the proper centrifugal pump to be selected.

To size the proper centrifugal pump the total amount of pressure drops for both purposes of the closed loop needed to be assessed. Based on the parameters that were varied in each purpose the largest pressure dropped achieved was in the first scenario at a pressure drop of 489.59 kPa (71.01 PSI), thus the pump was governed around that designed. The pump chosen was a Grundfos CM15-2 A-S-G-E-AQQEEAN. This pump can pump up to 340 liters/min (89.8 gallons/min) with a maximum operating pressure of 999.74 kPa (145 PSI). Sub components were later chosen to complete the assembly of loop, these components were, flow meter, expansion tank, thermocouple, fluid filter, and pipe fittings. All the equipment was built and assembled on a moveable cart made from strut channels with dimensions of 2.7 feet width x 6 feet height x 5.1 feet length. The cart has casters on the bottom to make it easily portable when moving around the test facility. The cart was lined with a thick Aluminum sheet of metal for structural support for the equipment and for ease of implementation of the equipment. Loop was constructed with the help of the Biological and Agricultural Engineering shop at the University of California Davis, a Post-Doctoral employee in the lab, and myself.

Test Facility Description

Heat absorbed into the Fluid
This method is one of two steps used to characterize the efficiency at the focal point for the microchannel and commercial receiver. This process was used to assess how much energy is transferred to the working fluid from the commercial receiver and in later experiments from the microchannel receiver. The fluid used in this loop is water. During on sun test the actual amount of solar energy that is collected is assessed with readings from the inlet and exit of the thermocouples and the flowmeter. Using this data, it shows the amount of solar energy that is collected during the testing period. With this data the average of the amount of flux was taken over that testing period giving a value that will be used to calculate the efficiency.

Heat Rate Incident on Receiver

The second method used, helped to characterize the amount of energy incident at the focal of the receiver surface using Sandia Phlux mapping tool [7]. This program uses images taken from the

receiver and sun during on sun tests and creates a flux map distribution of the amount of solar energy incident on the surface of the receiver. To obtain the flux map a few parameters were required. First was a digital image of the illuminated receiver and the sun with the corresponding filter factor that was applied to the camera. Next a current reading of the direct normal irradiance (DNI) that corresponds to the day the sun and receiver image was taken. Lastly the receiver reflectivity, the distance from the base of the receiver, and the angle formed with the camera to the base of the receiver [7]. To assess the uncertainty in the flux determined by the PHLUX program six parameters were varied and information on the filter lens for the camera taking the images. The six parameters were broken up into six cases that were adjusted. First case was the solar incident on the receiver case A, the reflectivity of the surface case B, the distance the image was taken from the receiver case C, receiver image control volume case D, and suns control volume case E. Each parameter was varied while the others were held constant to determine how each one affects the amount of solar incident on the receiver. Table 1 shows a list of the varied values for each parameter in each case.

Table 1: Parameters for each trial:

	Solar Incident (Watts/m^2)	Receiver Reflectivity	Distance (m)	Angle of Camera (degrees)
Trial 1	647.77	.79	10.8	39.7
Trial 2	630	.81	10.9	39.7
Trial 3	635.81	.83	11.0	39.7
Trial 4	641.05	.85	11.1	39.7
Trial 5	620	.87	11.2	39.7
Trial 6	660	.9	11.3	39.7
Base Values	647.77	.79	11	39.7

To obtain the output a base case for all the parameters was established seen in Table 1. The base case will be used for later uncertainty analysis. Using the images captured they are uploaded into the Sandia PHLUX program. The next step was to draw a control volume around the receiver and sun image, to indicate to the program what is the main area of focus. The receiver control volume will be an ellipse shape while the sun control volume will be a circle. Table 2 and 3 shows the coordinates of the receiver and sun image. When selecting the control volume, it is essential to draw the region with Sandia cropping tool closely around your region of interest making the region too large can skew the output results.

Table 2: Receiver Control Volume

	Square Cross Section (pixels)		Ellipse Cross Section (pixels)		
	Point 1 (x,y)	Point 2 (x,y)	Point 1(x,y)	Point 2 (x,y)	Axis Length
Trial 1	610,281	465,420	496,315	577,382	182
Trial 2	608,279	463,422	494,317	577,384	184
Trial 3	613,277	460,424	494,312	579,386	186
Trial 4	615,274	458,427	491,310	582,389	187
Trial 5	618,272	455,429	489,308	582,391	189
Trail 6	620,269	453,432	491,305	582,393	192

Table 3: Sun Control Volume

	Circle Control Volume (pixels)		
	Point 1(x,y)	Point 2 (x,y)	Axis Length
Trial 1	587,274	646,393	133
Trial 2	584,274	646,396	136
Trial 3	582,272	649,396	141
Trial 4	584,272	646,396	139
Trial 5	587,272	646,398	140
Trail 6	587,274	646,398	138

To assess the amount of flux on the main region of interest the two files used were the txt file on the transects of the receiver ellipse control volume and the MATLAB file. Using a filter function in MATLAB majority of the noise was removed. The image was refined more using a series of test to find the optimal filter value which removed majority of the noise and produced a cleaner image. From the test it showed that any matrix cell below 1.8e5 W/m2 was removed from the matrix leaving mostly the region of interest within the matrix. Fig. 7 and Fig. 8 shows a comparison before and after the filter factor was applied.
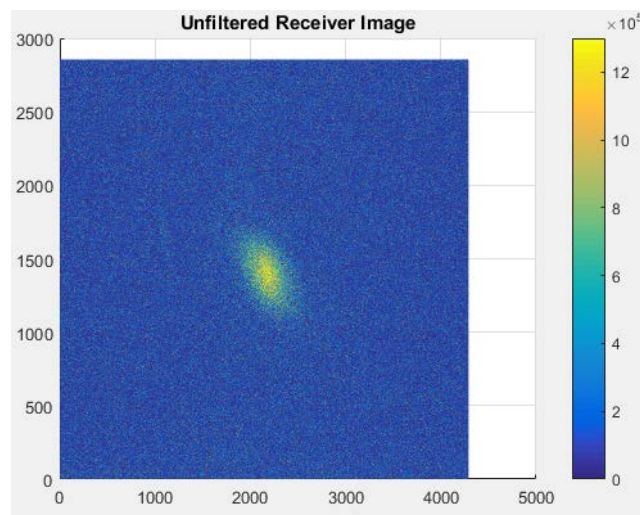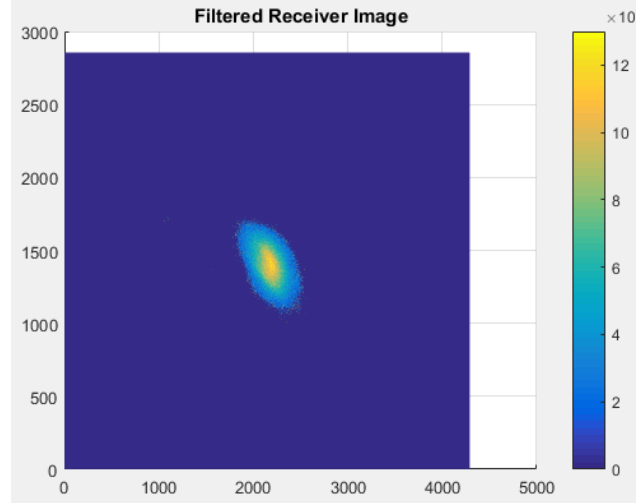

Figure 7: Unfiltered Image

Figure 8: Filter Image at 1.8E5

Using the transect file and the actual dimensions of the commercial receiver a conversion factor is created to convert pixels to meters and the differential spacing in the x and y direction in relation to each pixel. By taking the conversion factor and the differential spacing it was applied it to each individual cell in the MATLAB model the total amount of watts incident on the receiver surface is assessed. This was done by finding the differential area using x and y spacing. Applying the differential area to each cell within the matrix the cells are now in terms of watts, summing up each individual cell produces the total amount of flux incident on the receiver. Repeating this process for each case shows how the parameters affects the amount of flux. Using the information from heat absorbed by the fluid and the information from the solar energy incident on the receiver surface the efficiency was solved. The equation used to solve this is described as

Equation 7: $\eta_{reciever} = \dfrac{q_{fluid}}{q_{incident}}$

Results:

Based on the results for the heat absorbed by the fluid Fig. 9 shows that over the span of time amount of energy to the fluid increased until it reached steady states. From the experiment it took approximately 40 minutes to reach steady state conditions. Taking the average of the amount of heat flux for the steady state region gave the data used for further calculations. The average absorbed heat for that region was 18.65 kW (25 hp). The results from this experiment showed that heat absorption by the fluid is in agreement with what it should be. The manufacturer data showed that the parabolic dish with the commercial receiver can achieve up to 25 kW (33.5 hp) of heat absorption to the working fluid at 1000 sun energy concentration. Results showed that the value was around 19 kW (25.47 hp). Though slightly lower, the data was still close to manufacture data because the amount of Direct Normal Irradiance (DNI) for that day was lower compared to what the manufacture claimed. The lower DNI percentage at which the experiments

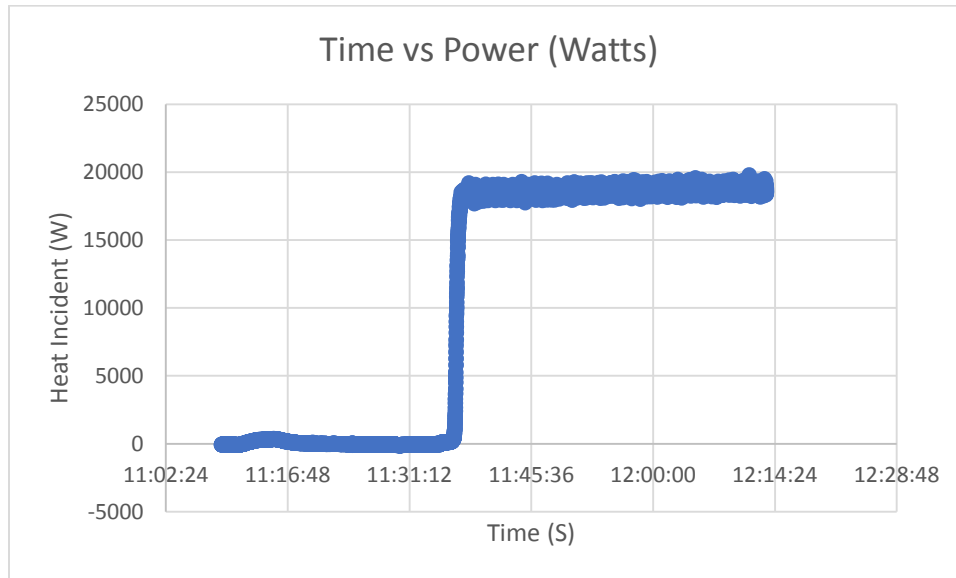were conducted matches with the expected amount of solar energy that should be incident on the receiver.

Figure 9: The variation of absorbed heat by the working fluid over testing period

For the heat rate incident on the receiver the results can be seen in Table 4 and Table 5 for a filter factor of 1.71e5 watts/m^2 and 1.8e5 watts/m^2 respectively. The data shows how the results for each parameter affected the calculated solar radiation. Case A was varying the solar flux, Case B was adjusting the reflectivity of the receiver surface, Case C was taken by varying the distance the camera picture was taken from the receiver, and Case D and E was adjusting the receiver and sun image control volume in the program. In Case A, seen in Table 4 and 5, increasing the amount of solar heat flux lead to increase in the total amount of solar energy incident on the receiver. In Case B by increasing the reflectivity starting from 0.79 to 0.90, it shows that there is smaller amount of absorbed solar energy. For Case C the distance that the picture was taken from the receiver didn't have a significant effect on the output data. In CASE D the data shows that varying the size of the control volume can have noticeable changes to the result. This shows how sensitive the control volume was to the slight changes and the importance of keeping it consistent as possible. The same trend was seen in Case E when adjusting the suns control volume. For future experiments the control volume for both CASE E and CASE D has to be looked at with close care to ensure it doesn't alter the results.

Table 4: Total Watts (W) at Filter of 1.71e5 watts/m^2

	CASE A	CASE B	CASE C	CASE D	CASE E
Trial 1	24271	26666	24014	26493	20932
Trial 2	23337	25704	24271	25607	22287
Trial 3	23552	24906	24271	2427	24271
Trial 4	22587	24271	24271	22658	23277
Trial 5	22893	23443	24271	21716	23525
Trail 6	24779	22522	24271	21178	22724

The UC Davis McNair Scholars Journal

Table 5: Total Watts (W) at Filter of 1.8e5 watts/m^2

	CASE A	CASE B	CASE C	CASE D	CASE E
Trial 1	23846	26167	23594	26030	20604
Trial 2	23089	25412	23846	25159	22025
Trial 3	23339	24573	23846	23846	23846
Trial 4	22257	23846	23846	22262	23030
Trial 5	22554	23231	23846	21336	23312
Trail 6	24448	22193	23846	20808	22455

Once all the input parameter values are established the Sandia PHLUX program outputs several files used to assess the solar incidence. The files are images of a flux map of the control volume that was selected as seen in Fig.10, with a color indicating the amount of flux received by each pixel, an image of the whole receiver seen in Fig. 11, sun image seen in Fig. 12, Irradiance profile of the sun image, and irradiance plot along the vertical and horizontal transects of the receiver as seen in Fig. 13. The next set of files that the Sandia program produces was a txt files of the flux along the transects lines of the receiver image, the second file described the normalize ring irradiance for the sun effective radius from the centroid, and the last file was a MATLAB file of the flux distribution (W/m^2) across the whole receiver image for each pixel.
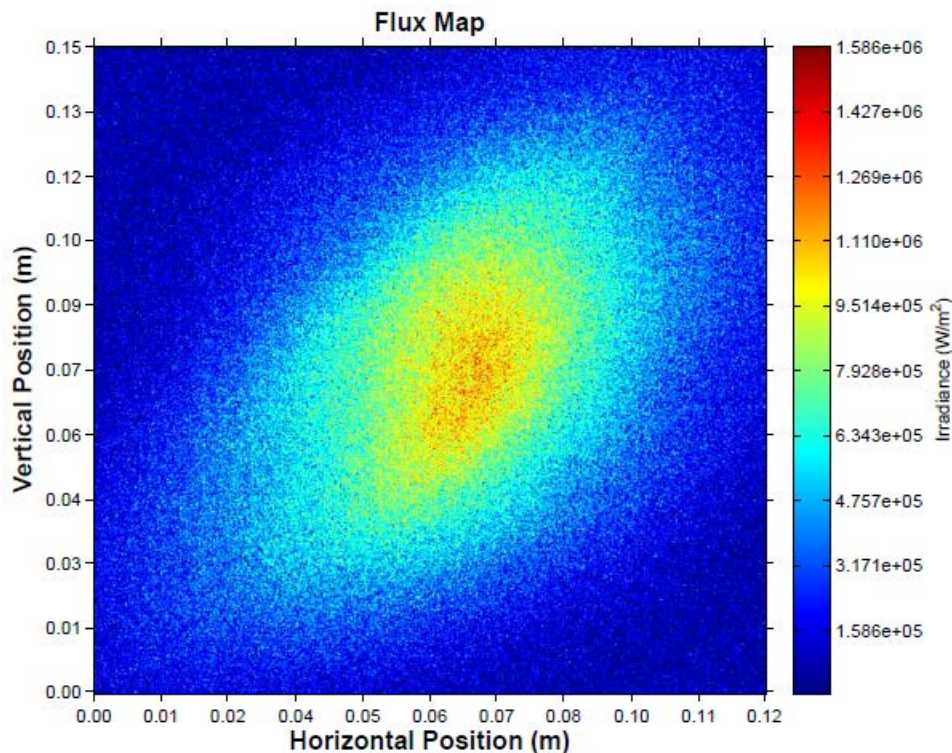

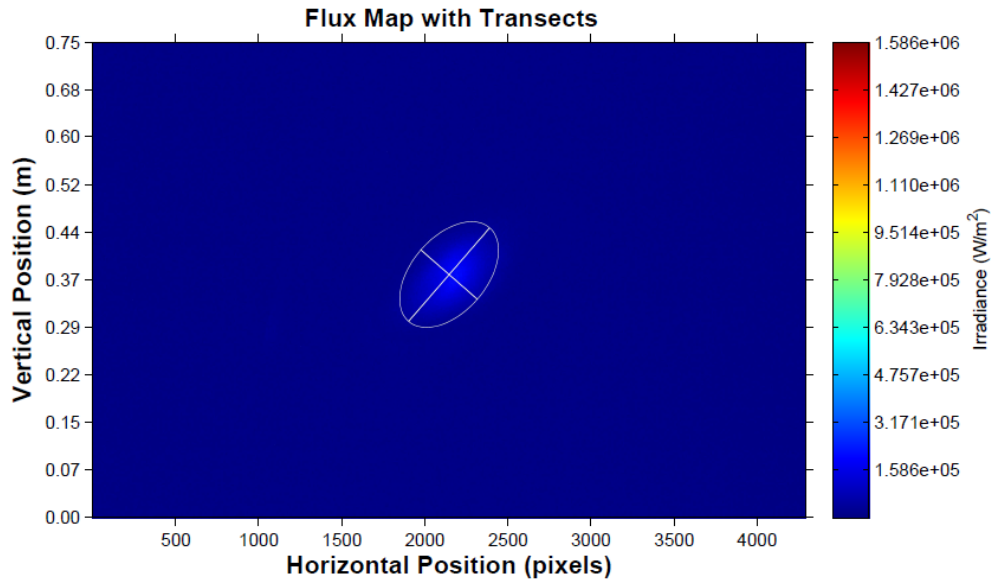Figure 10: Flux map of the irradiance for receiver region or interest

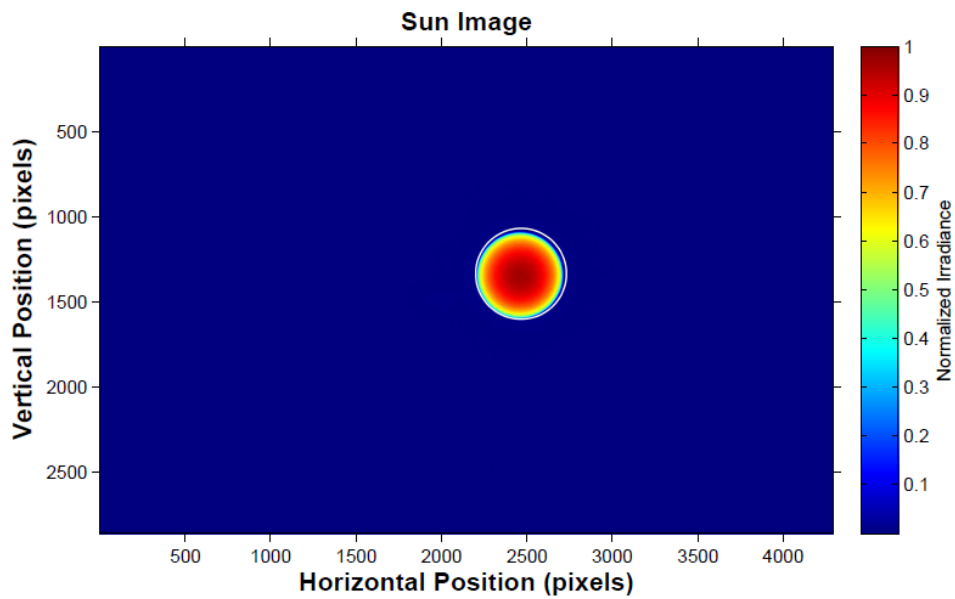Figure 11: Image of receiver control volume with Transects

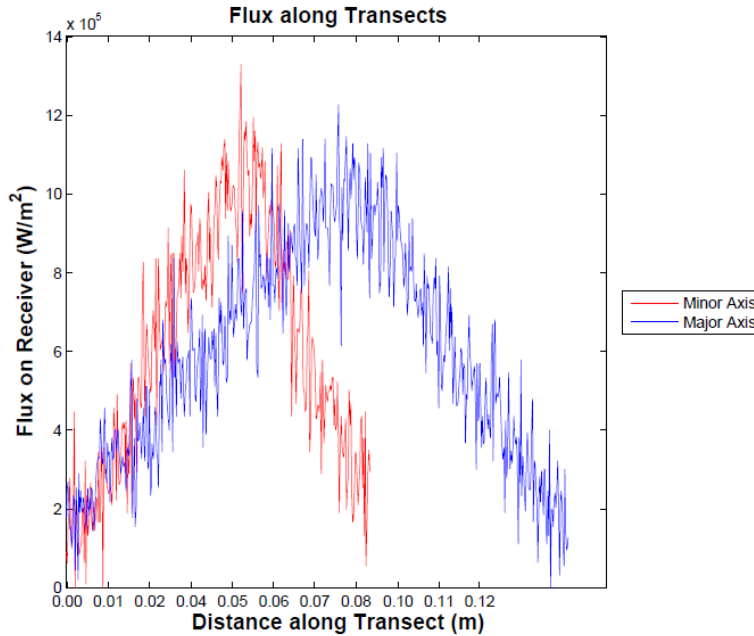Figure 12: Image of sun with control volume

Figure 13: Plot of the transects for receiver control volume

Using the results obtained from the heat absorbed by the fluid and the solar energy incident on the receiver surface, Equation 7 was used to assess the efficiency the results can be seen in Table 6 and 7. Most cases the average efficiency was around the 80 percentiles. Uncertainty calculations can be seen in Table 8 for both filter factors.

Table 6: Efficiency at Filter of 1.71e5 watts/m^2

	CASE A	CASE B	CASE C	CASE D	CASE E
Trial 1	0.768	0.699	0.776	0.703	0.891
Trial 2	0.799	0.725	0.768	0.728	0.836
Trial 3	0.791	0.748	0.768	0.768	0.768
Trial 4	0.825	0.768	0.768	0.823	0.801
Trial 5	0.814	0.795	0.768	0.858	0.792
Trail 6	0.752	0.828	0.768	0.880	0.820
Average	0.79	0.76	0.77	0.79	0.82

Table 7: Efficiency at Filter of 1.8e5 watts/m^2

	CASE A	CASE B	CASE C	CASE D	CASE E
Trial 1	0.782	0.712	0.790	0.716	0.905
Trial 2	0.807	0.733	0.782	0.741	0.846
Trial 3	0.799	0.758	0.782	0.782	0.782
Trial 4	0.837	0.782	0.782	0.837	0.809
Trial 5	0.826	0.802	0.782	0.874	0.800
Trail 6	0.762	0.840	0.782	0.896	0.830
Average	0.80	0.77	0.78	0.80	0.83

17

Using the information provided from both process, perturbation uncertainty analysis was performed on the results to assess errors within the calculation. To calculate the uncertainty first there needed to be a base case established. The perturbation error analysis considers the effect of input tolerances on the output flux from the program. Uncertainty in the parameters measured were obtained by combining output data in a root-sum-square manner, with the use of excel. Results of the uncertainty of the output data can be seen in Table 8:

Table 8: Uncertainty for Filter of 1.71e5 watts/m^2 & 1.8e5 watts/m^2

	Filter 1.71e5	Filter 1.8e5
Uncertainty in q	3545	3411
% Uncertainty	14.60	14.30

Conclusion:

An experimental and data analysis framework was developed to assess the efficiency of solar thermal receiver in this paper. Using the amount of energy transferred to the working fluid and the amount of solar energy incident on the receiver surface with Sandia PHLUX mapping program, help provide a proper way to calculate efficiency. From the result, the data showed the commercial receiver had an efficiency around 80 %. After calculations were finished Perturbation uncertainty analysis was used to assess the uncertainty in the results. Once completion of the sCO$_2$ loop is finalized the newly designed microchannel receivers' efficiency will be assessed. Using the method presented in this paper to calculate the commercial receiver the same process can be done for the microchannel to assess its performance and other newly design receivers in the future.

Reference:

[1] Department of Energy. Office of Energy Efficiency & Renewable Energy (2011). DOE Pursues SunShot Initiative to Achieve Cost Competitive Solar Energy by 2020. Sunshot initiative

[2] Ho C., <u>Advances in central receivers for concentrating solar application</u>, Solar Energy Volume 152, 2017,Pages 38-56,

[3] L'Estrange T, Truong E., Rymal C., Rasouli E., Narayanan V., Apte S., Drost K., <u>High Flux Microscale Solar Thermal Receiver for Supercritical Carbon Dioxide Cycles,</u> ASME 2015 13th International Conference on Nanochannels, Microchannels, and Minichannels, ICNMM 2015, collocated with the ASME 2015 International Technical Conference and Exhibition on Packaging and Integration of Electronic and Photonic Microsystems

[4] SOLARTRON ENERGY SYTEM INC. Absorber Box: *Assembly Drawing*. Ambherst, Nova Scotia, Canada: SOLARTRON.

[5] SOLARTRON ENERGY SYSTEM INC. Solar Concentrator: *Datasheet*. Ambherst, Nova Scotia, Canada: SOLARTRON.

[6] EMMEGI HEAT EXCHANGERS, INC. Heat Exchanger: Data Sheet. Phoenix, AZ, Rick Dodd.

[7] Ho CK, Khalsa SS. A Photographic Flux Mapping Method for Concentrating Solar Collectors and Receivers. ASME. J. Sol. Energy Eng. 2012;134(4):041004-041004-8. doi:10.1115/1.4006892.

[8] Rymal C., Apte S., Narayanan V., Drost K. (2013), <u>Numerical Design Of A High-Flux Microchannel Solar Receiver</u>, ASME 2013 7th Int. Conf. on Energy Sustainability Collocated with the ASME 2013 Heat Transfer Summer Conf. and the ASME 2013 11th Int. Conf. on Fuel Cell Science, Engineering and Technology, ES 2013, art. no. V001T11A012

[9] Zada K., Hyder M., Drost K., Fronk B., <u>Numbering- Up of Microscale Devices for Megawatt-Scale Supercritical Carbon Dioxide Concentrating Solar Power Receivers</u>, Journal of Solar Energy Engineering, Transactions of the ASME (2016), Volume 138, Issue 6.

[10] Bradshaw R.W., Meeker D.E., <u>High-temperature Stability of Ternary Nitrate Molten Salts for Solar Thermal Energy Systems</u>, Solar Energy Materials (1990), Issue 1, Pg 51-60

[11] Gobereit B., Amsbeck L., Buck R., Pitz-Paal R., Roger M., Muller-Steinhagen H., <u>Assessment of a Falling Solid Particle Receiver with Numerical Simulation</u>, Solar Energy (2015), Volume 115, Page 505-517

[12] Zunft S., Hanel M, Kruger M., Gohring F., Wahl E., <u>Julich Solar Power Tower Experimental Evaluation of the Storage Subsystem and performance Calculation</u>, Journal of Solar Energy Engineering (2011), Transactions of the ASME,Volume 133

[13] Besarati SM, Yogi Goswami DD, Stefanakos EK. Development of a Solar Receiver Based on Compact Heat Exchanger Technology for Supercritical Carbon Dioxide Power Cycles. ASME. J. Sol. Energy Eng. 2015;137(3):031018-031018-8. doi:10.1115/1.4029861.

[14] Clifford K. Ho. A Review of High-Temperature Particle Receivers for Concentrating Solar Power. Applied Thermal Engineering, Volume 109, Part B, 2016, Pages 958-969, ISSN:1359-4311

[15] Clifford K. Ho, Joshua M. Christian, Julius Yellowhair, Nathan Siegel, Sheldon Jeter, Matthew Golob, Said I. Abdel-Khalik, Clayton Nguyen, Hany Al-Ansary, On-Sun Testing of an Advanced Falling Particle Receiver System, American Institute of Physic Conference Proceedings, Volume 1734, 2016

[16] NREL. (2017, March 20). *Planta Solar 10*. Retrieved from https://www.nrel.gov/csp/solarpaces/project_detail.cfm/projectID=38

[17] NREL. (2017, March 20). *Planta Solar 20.* Retrieved from https://www.nrel.gov/csp/solarpaces/project_detail.cfm/projectID=39

[18] NREL. (2014, March 10). *Ivanpah Solar Electric Generating System*. Retried from https://www.nrel.gov/csp/solarpaces/project_detail.cfm/projectID=62